Available online at www.sciencedirect.com
ScienceDirect
Trans. Nonferrous Met. Soc. China 35(2025) 2372−2385
Transactions of Nonferrous Metals Society of China
www.tnmsc.cn

# New molybdenum metallurgy process based on water-soluble mineral phase conversion of molybdenite

Mu-ye CUI[1], Jiang-tao LI[1,2], Zhong-wei ZHAO[1,2], Xu-heng LIU[1], Xing-yu CHEN[1], Li-hua HE[1], Feng-long SUN[1]

1. School of Metallurgy and Environment, Central South University, Changsha 410083, China;
2. Key Laboratory of Hunan Province for Metallurgy and Material Processing of Rare Metals, Central South University, Changsha 410083, China

Received 28 November 2023; accepted 30 August 2024

**Abstract:** Potassium hydroxide (KOH) was introduced into the molybdenite roasting process to convert molybdenum (Mo) and sulfur (S) into water-soluble potassium molybdate ($K_2MoO_4$) and potassium sulfate ($K_2SO_4$). Roasting with a 1.8-fold excess of KOH at 400 °C for 3 h enabled the leaching of over 99% of Mo from the molybdenum calcine using water. A precipitation method involving potassium–magnesium (K−Mg) salts was proposed for impurity removal. Under the conditions of pH 11, 30 °C, excess coefficient of 1.7 for Mg salts, and a duration of 1 h, 98.37% of phosphorus (P) was removed from the $K_2MoO_4$ solution. With post-purification, over 99% of Mo crystallized upon adjustment of pH to 1. Subsequently, S and K were recovered as $K_2SO_4$ fertilizer from the crystalline mother liquor. An environmentally sustainable approach was proposed to conduct molybdenite production and ensure the efficient recovery of both Mo and S.

**Key words:** molybdenite; sulfur fixation roasting; magnesium potassium phosphate; potassium polymolybdate

## 1 Introduction

Molybdenum (Mo), a crucial rare metal, has extensive application in steel, petrochemical, and aerospace industries [1]. Molybdenite ($MoS_2$) is the principal mineral resource for Mo [2,3], and it is conventionally processed via oxidative roasting. The high sulfur (S) content in $MoS_2$ (>20%) leads to exothermic reactions during the oxidation [4]. Temperatures exceeding 700 °C can accelerate the sublimation of molybdenum oxide products, necessitating substantial air intake to regulate furnace conditions. This often results in the emission of low-concentration sulfur dioxide ($SO_2$) flue gas (3% in fluidized bed roasters, 0.8%−3% in multiple hearth furnaces, and 0.8%−2% or higher in rotary kilns) [5]. The low $SO_2$ concentration complicates acid production and poses challenges related to excessive $SO_2$ emissions. Oxidative roasting yields Mo calcite, which is typically processed via ammonia leaching to produce ammonium molybdate [6]. However, impurities such as copper (Cu), iron (Fe), and calcium (Ca) form insoluble molybdates during roasting, often result in low Mo leaching efficiency under weak alkali ammonia conditions [7−9].

To mitigate $SO_2$ emissions, additives such as soda [10] or lime [11] have been employed during roasting. Lime not only converts $SO_2$ into calcium sulfate but also forms insoluble calcium molybdate, which requires a substantial sodium leaching agent for Mo extraction. Sodium carbonate addition converts Mo and S into soluble salts but produces sodium sulfate and ammonia nitrogen waste-water during subsequent ammonium molybdate purification, thereby posing treatment challenges. Recent studies have focused on the molybdenite

**Corresponding author:** Jiang-tao LI, Tel: +86-731-88830476, E-mail: jiangtao-lee@csu.edu.cn
https://doi.org/10.1016/S1003-6326(25)66821-X

hydrometallurgy, including nitric acid leaching [12], pressure acidic/alkaline leaching [13,14], sodium hypochlorite/dichromate leaching [15], and electrochemical leaching [16]. These methods often require high temperatures, pressures, and chemical dosages to achieve efficient Mo extraction due to the unique crystal structure, stable chemical properties, and superior $MoS_2$ hydrophobicity [17]. However, these approaches frequently result in high chemical consumption, high equipment costs, extensive sulfate wastewater, and challenging wastewater treatment [18,19].

To address these challenges, in this study, the addition of potassium hydroxide (KOH) during oxidative roasting was explored to convert $MoS_2$ into soluble $K_2MoO_4$ and $K_2SO_4$. Furthermore, the $K_2SO_4$ produced is a readily recoverable raw material for agricultural fertilizers, effectively utilizing S resources [20−22]. The potassium (K) salt system, akin to conventional ammonium salt systems due to the similar $K^+$ and $NH_4^+$ radii, simplified purification and extraction. Therefore, a potassium–magnesium (K−Mg) salt precipitation method was compared with the conventional ammonium−magnesium salt precipitation method for impurity removal. The acidizing crystallization process leveraged the minimal solubility of poly-potassium molybdate ($K_2MoO_4$) to extract Mo. Additionally, K addition during ammonium molybdate preparation enhanced the K content, meeting requirements for downstream Mo processing enterprises [23−26]. Therefore, this study would offer a technical approach for preparing potassium-doped ammonium molybdate.

## 2 Experimental

### 2.1 Materials

To explore the reaction mechanism in this experiment, a high-grade molybdenite #1 was obtained from Yichun, Heilongjiang Province, China. The X-ray fluorescence (XRF) spectral data of this molybdenite #1 are presented in Table 1, which indicates that the raw material contained 56.6% Mo and 38.16% S. Furthermore, X-ray diffraction (XRD) was employed to characterize the molybdenite #1. As shown in Fig. 1, the raw material was $MoS_2$ with a small amount of gangue. Additionally, another high-grade molybdenite #2 containing high phosphorous (P), arsenic (As), and silicon (Si) impurities was obtained with its XRF spectral data presented in Table 1. Both types of molybdenite were ground to relatively fine particles (<75 μm) after washing, drying, and grinding using a vibrating mill. The agents utilized, including KOH, $MoO_3$, $K_3PO_4$, and $MgSO_4$ were of analytical

**Table 1** XRF data of two types of molybdenite (wt.%)

| Element | Molybdenite #1 | Molybdenite #2 |
|---|---|---|
| Mo | 56.61 | 46.68 |
| S | 38.16 | 28.97 |
| Bi | 1.74 | |
| O | 1.10 | 13.50 |
| Pb | 1.03 | 0.05 |
| Si | 0.42 | 2.32 |
| Fe | 0.24 | 2.22 |
| Al | 0.13 | 0.57 |
| W | 0.11 | |
| K | 0.11 | 0.26 |
| Cu | 0.09 | 0.95 |
| Ca | 0.06 | 0.89 |
| Ag | 0.06 | |
| Se | 0.04 | 0.03 |
| Mn | 0.04 | 0.01 |
| Mg | 0.04 | 2.68 |
| Cr | 0.02 | |
| Zn | 0.01 | 0.03 |
| P | | 0.05 |
| As | | $8.13\times10^{-5}$ |
| Cl | | 0.09 |
| Ti | | 0.05 |

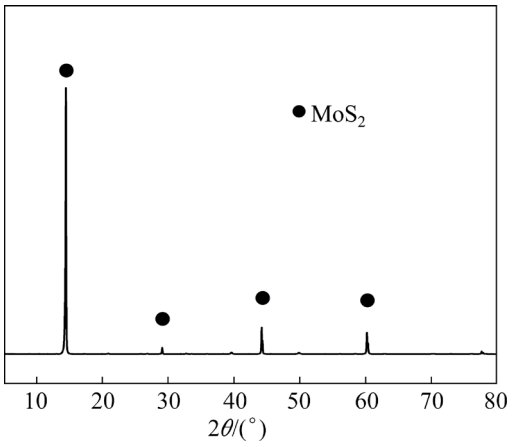


**Fig. 1** XRD pattern of molybdenite #1

reagent grade and purchased from Sinopharm Chemical Reagent Co., Ltd. Additionally, $H_2SO_4$ (≥98.08%) was purchased from the Hengyang Kaixin Chemical Reagent Co., Ltd. All aqueous solutions were prepared with deionized water.

### 2.2 Methods

A schematic diagram of the experimental process is shown in Fig. 2. Molybdenite and KOH were slurried to the concentration required for the experimental conditions and subsequently added to a 100 mm × 50 mm × 30 mm porcelain boat. The boat was then placed in a high-temperature pit furnace and heated to different temperatures with sufficient oxygen. After roasting, the roasting slag was transferred into a beaker with deionized water at 90 °C for 2 h, filtered, and separated. Subsequently, the residue was washed several times with deionized water, dried in an oven at 80 °C for 12 h, and then weighed. Finally, the Mo content of the leaching residue and leachate was analyzed through inductively coupled plasma optical emission spectroscopy combined with the fusion method. The corresponding leaching efficiency ($\eta_1$) was then calculated using Eq. (1):

$$\eta_1 = \frac{c_1 \cdot V_1}{m_1 \cdot w_1} \times 100\% \tag{1}$$

where $m_1$ is the mass of molybdenite (g), $w_1$ denotes the Mo content in the ore, $c_1$ represents the Mo concentration in the leaching solution (g/L), and $V_1$ signifies the volume of the leaching solution (L).

To simulate a molybdenum-leaching solution, 1 mol/L solution of pure $K_2MoO_4$ was prepared through a solid–liquid reaction to simulate a molybdenum-leaching solution. Subsequently, $MgSO_4$ was added to the reaction at a special temperature, and the pH of the solution was kept above and below the target pH throughout the process. The mixture was stirred in a constant-temperature water bath to facilitate the removal reaction. The resulting precipitate was separated through filtration and dried in an oven. The removal efficiency of P ($\eta_2$) and Mo loss ratio ($\eta_3$) were calculated using Eq. (2) and Eq. (3), respectively:

$$\eta_2 = \left(1 - \frac{c_3 \cdot V_3}{c_2 \cdot V_2}\right) \times 100\% \tag{2}$$

$$\eta_3 = \left(1 - \frac{c_5 \cdot V_5}{c_4 \cdot V_4}\right) \times 100\% \tag{3}$$

where $c_2$ and $c_3$ are the concentrations of P in the leaching solution and the purified solution (g/L), respectively; $V_2$ and $V_3$ are the volumes of the leaching solution and purified solution (L), respectively; $c_4$ and $c_5$ are the concentrations of Mo in the leaching solution and the purified solution (g/L), respectively; $V_4$ and $V_5$ are the volumes of the leaching solution and purified solution (L), respectively.

The pH of the purified molybdate–potassium sulfate solution was adjusted, and the acidic precipitation crystallization was conducted to obtain $K_xMoO_4$ crystals. The crystallization efficiency ($\eta_4$) and the residual Mo ($\eta_5$) were calculated using Eq. (4) and Eq. (5), respectively:

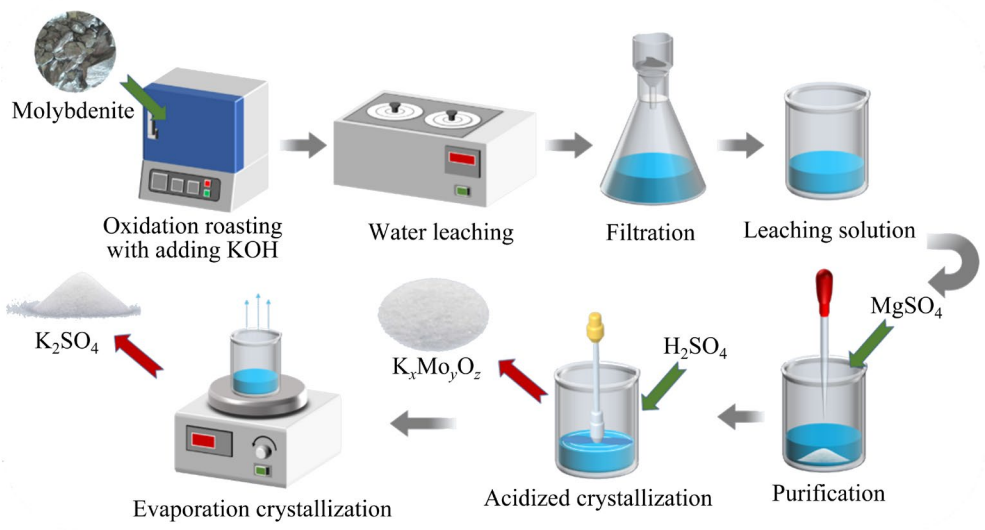


**Fig. 2** Schematic diagram for molybdenum recovery from molybdenite

$$\eta_4=\left(1-\frac{c_7\cdot V_7}{c_6\cdot V_6}\right)\times 100\% \quad (4)$$

$$\eta_5=\frac{c_7\cdot V_7}{c_6\cdot V_6}\times 100\% \quad (5)$$

where $c_6$ and $c_7$ are Mo concentrations in the purified solution and solution after crystallization (g/L), respectively; $V_6$ and $V_7$ are the volumes of the purified solution and the solution after crystallization (L), respectively.

## 3 Results and discussion

### 3.1 Oxidative roasting with KOH addition

3.1.1 Roasting mechanism

Most Mo-deep processing enterprises require K addition to enhance Mo performance, mainstreaming ammonium molybdate products. The ammonium molybdate products, commonly utilized in the industry, impose strict broad limits on K impurity content. As a strong base, KOH not only reacted thoroughly with roasted molybdenum trioxide products but also effectively absorbed $SO_2$. Consequently, this reaction converted $MoS_2$ into soluble $K_2MoO_4$ and $K_2SO_4$, addressing $SO_2$ emissions and optimizing S resource utilization.

Analysis of the thermodynamic properties and oxidation laws of molybdenite offered a theoretical basis and valuable insights into oxidative roasting. The chemical equations within the Mo−S−O system and the calculated reaction-free energy variables at different temperatures according to available thermodynamic data are presented in Table 2 [27].

**Table 2** Chemical reactions and free energy variables in Mo−S−O system

| Number | Reaction | $\Delta G_m^\theta(T)$/(kJ·mol$^{-1}$) | |
|---|---|---|---|
| | | 500 K | 700 K |
| 1 | $MoS_2+3O_2(g)=MoO_2+2SO_2(g)$ | −838.085 | −809.936 |
| 2 | $MoO_2+0.5O_2(g)=MoO_3$ | −120.839 | −107.232 |
| 3 | $Mo+O_2(g)=MoO_2$ | −495.555 | −459.261 |
| 4 | $MoS_2+2O_2(g)=Mo+2SO_2(g)$ | −342.530 | −350.675 |
| 5 | $MoS_3+O_2(g)=MoS_2+SO_2(g)$ | −278.044 | −282.943 |
| 6 | $MoS_3+4O_2(g)=MoO_2+3SO_2(g)$ | −1116.129 | −1092.879 |
| 7 | $MoS_3+4.5O_2(g)=MoO_3+3SO_2(g)$ | −1236.968 | −1200.111 |

The reaction equilibrium constant ($K$) was calculated as

$$\lg K=-\Delta G_m^\ominus/(2.303RT) \quad (6)$$

For the following chemical reaction, its corresponding $K$ was

$$A+B+aO_2(g)=C+D+bSO_2(g) \quad (7)$$

$$K=(p_{O_2}^b/p_{SO_2}^a)\cdot p_0^{(a-b)} \quad (8)$$

Then,

$$\lg p_{SO_2}=(a/b)\lg p_{O_2}+((b-a)/b)\lg p_0+(1/b)\lg K \quad (9)$$

Furthermore, Fig. 3 shows the thermodynamic calculations, which shows $\lg p_{SO_2}-\lg p_{O_2}$ predominance-area diagrams for the Mo−S−O system at 500 and 700 K. Subsequently, as $p_{O_2}$ increased, it facilitated the conversion of $MoS_2$ to $MoO_3$. As the temperature increased from 500 to 700 K, the stable area of $MoO_2$ decreased, which indicated that increasing the temperature facilitated the complete Mo oxidation.

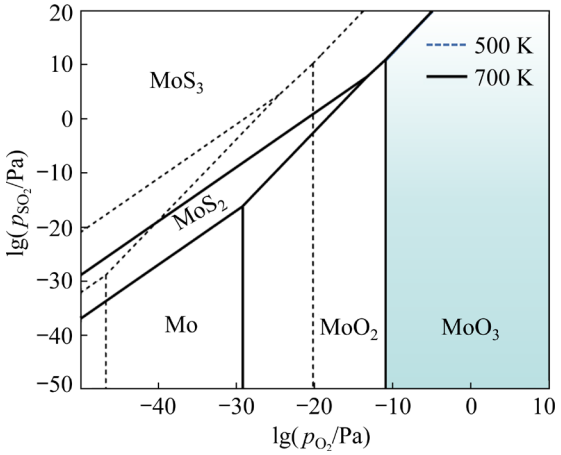


**Fig. 3** Predominance-area diagrams of Mo−S−O system

The primary reactions involving KOH during oxidative roasting are as follows:

$$MoO_3+2KOH=K_2MoO_4+H_2O \quad (10)$$

$$2MoO_2+O_2+4KOH=2K_2MoO_4+2H_2O \quad (11)$$

$$4KOH+2SO_2(g)+O_2(g)=2K_2SO_4+2H_2O \quad (12)$$

The corresponding standard Gibbs free energy ($\Delta G^\ominus$) versus the oxidation reaction temperature is shown in Fig. 4. It was observed that all reactions were theoretically feasible, with Reactions (11) and (12) exhibiting a greater tendency to occur compared with Reaction (10). As the oxidation temperature increased, $\Delta G^\ominus$ decreased for Reactions

(10) and (11), while that for Reaction (12) increased. This indicated that higher roasting temperatures facilitated the production of $K_2MoO_4$, but were unfavorable for the production of $K_2SO_4$. However, the very low $\Delta G^{\Theta}$ of Reaction (12) indicated that the tendency of the reaction to occur was largely disregarded. The thermodynamic calculations were correlated with the experimental results, further demonstrating the feasibility and rationality of performing oxidative roasting at 700 K.

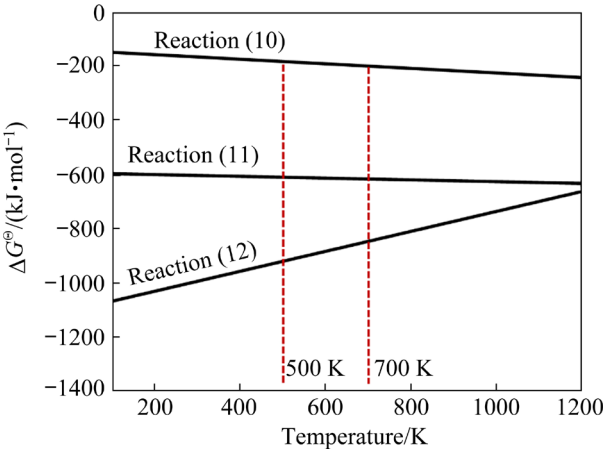


**Fig. 4** Thermodynamic results of oxidative roasting process of molybdenite

The X-ray photoelectron spectroscopy (XPS) spectra of molybdenite roasting products under the oxygen-enriched and low-oxygen conditions, including their chemical valences, are shown in Fig. 5. Quantification of S and Mo valence states on each sample was achieved through peak area fitting. Multiple S valence states were identified according to binding energies, with a notable higher proportion of low-valence S fraction under low-oxygen conditions, with $MoS_2$ accounting for 30.27% (Fig. 5(b)). Furthermore, Mo exhibited three valence states. However, precise attribution of Mo peaks at 226−232 eV was challenging due to overlapping of Mo 3d and S 1s peaks (Fig. 5(c)). Some Mo peaks in S-rich environments appeared near both $MoO_2$ and $MoS_2$ peaks [28]. The XPS spectra revealed an S-rich environment, and the XPS analysis was correlated with thermodynamic predictions, indicating that increased $p_{O_2}$ facilitated molybdenite conversion and sulfate formation [29].

3.1.2 Effect of oxidative roasting conditions on Mo extraction

The influence of oxidative roasting parameters on leaching was investigated, and we focused on the roasting temperature, KOH excess coefficient, and roasting time. In the experiment, molybdenite #1 was utilized, with leaching efficiency assessed under conditions similar to those in water leaching (Fig. 6). The leaching conditions included 2 h of leaching time, a temperature of 90 °C, and a liquid-to-solid ratio of 5∶1.

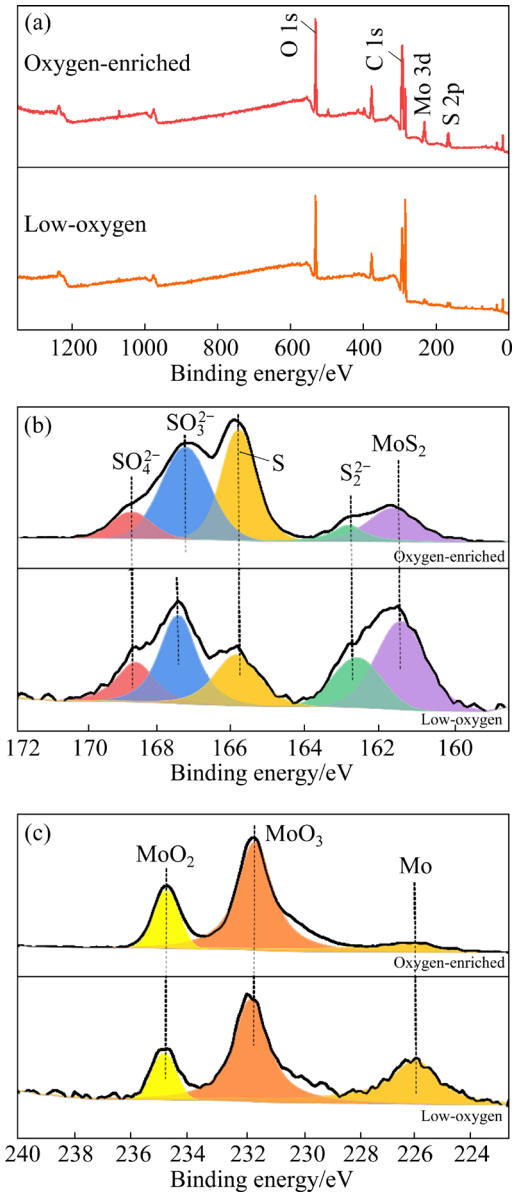


**Fig. 5** XPS spectra of roasting products at oxygen-enriched and low-oxygen conditions: (a) Survey XPS; (b) S spectrum; (c) Mo spectrum

The oxidative roasting temperature influenced Mo extraction significantly (Fig. 6(a)). At 400 °C, 93.71% of Mo was leached, while only 14.08% was leached at 200 °C. The XRD patterns of the molybdenum calcine before water leaching at 200 and 400 °C indicated that $SiO_2$ in the molybdenite

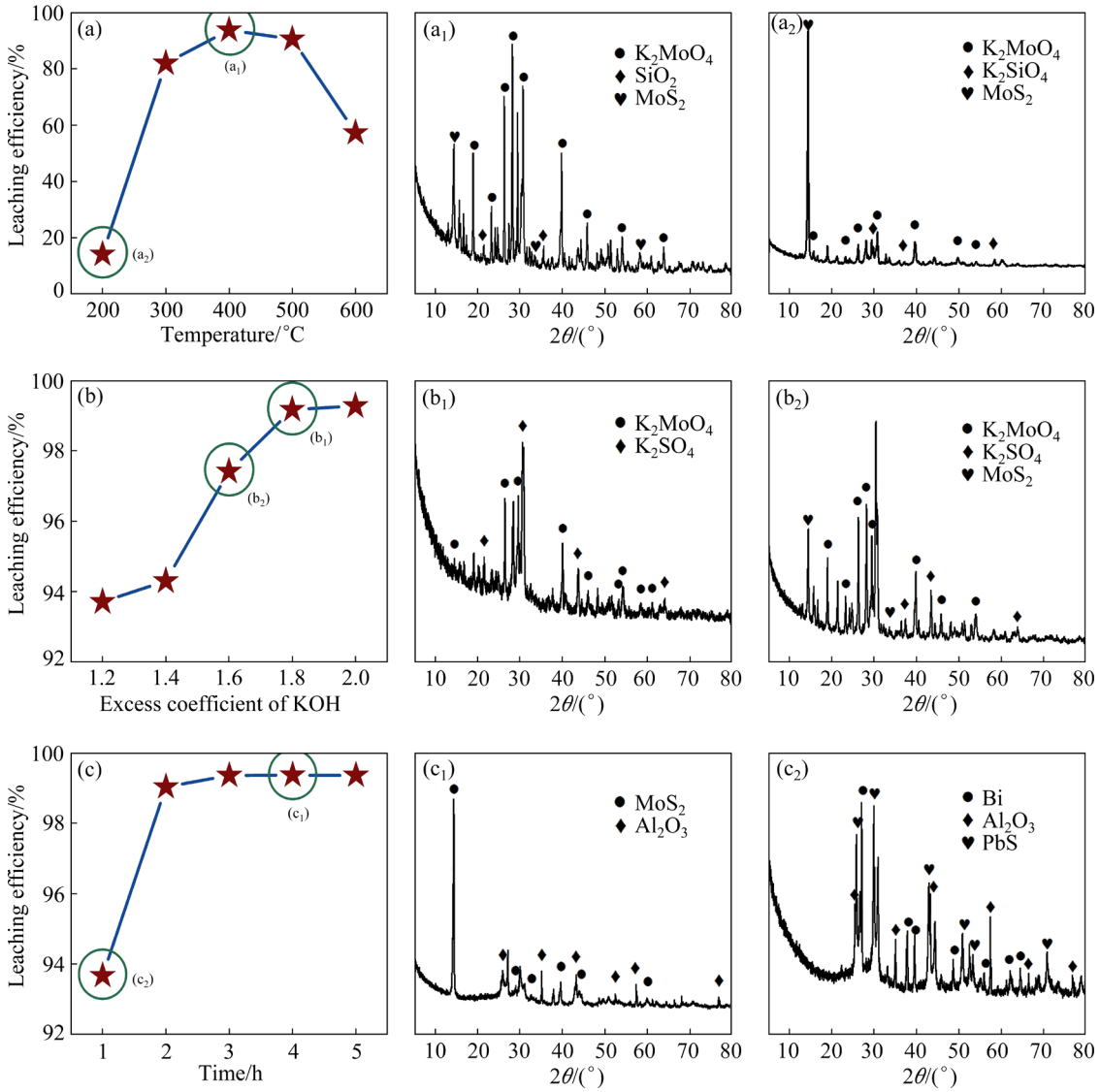


**Fig. 6** Effect of oxidative roasting conditions on leaching efficiency of Mo and XRD patterns of solid phase: (a, $a_1$, $a_2$) Temperature; (b, $b_1$, $b_2$) Excess coefficient of KOH; (c, $c_1$, $c_2$) Time

did not fully react at 200 °C, and $MoS_2$ was incompletely oxidized at different temperatures. Additionally, this indicated that the KOH excess coefficient of 1.2 was insufficient for complete Mo extraction. Furthermore, Fig. 6(b) shows the effect of the KOH excess coefficient on Mo leaching. The leaching efficiency of Mo increased as the excess coefficient increased from 1.2 to 2.0. The leaching efficiency of Mo reached 99.17% when the KOH excess coefficient reached 1.8. Beyond this point, further increase in KOH concentration had minimal impact on leaching efficiency, indicating that optimal oxidative roasting and subsequent leaching occurred at a KOH excess coefficient of 1.8 at 400 °C. The absence of $MoS_2$ phase in the material before water leaching under this condition indicated that almost all Mo elements entered the solution. The leaching efficiency also increased upon extending the roasting time. The leaching efficiency was stable at 99.35% after 3 h, which indicated a complete reaction under these conditions. Furthermore, increasing the roasting time further did not significantly affect the leaching efficiency. To balance the energy consumption in practical production, the roasting time was reduced to 2 h, ensuring effective leaching with appropriate temperature and alkali quantity. The XRD pattern in Fig. 6(c) showed that the solid phase remaining after 2 h of roasting and water leaching was primarily $MoS_2$, with no unreacted $MoS_2$ in the fully-roasted (4 h) water-leached residue. Only some Bi, $Al_2O_3$, $PbS_2$, and other gangue

components as well as impurities remained. Thus, the corresponding residual ratio was only 2.9%. Therefore, it was observed from the EDS of the water-leached residue shown in Fig. 7 that the impurities of Al and Si were enriched into the residue.

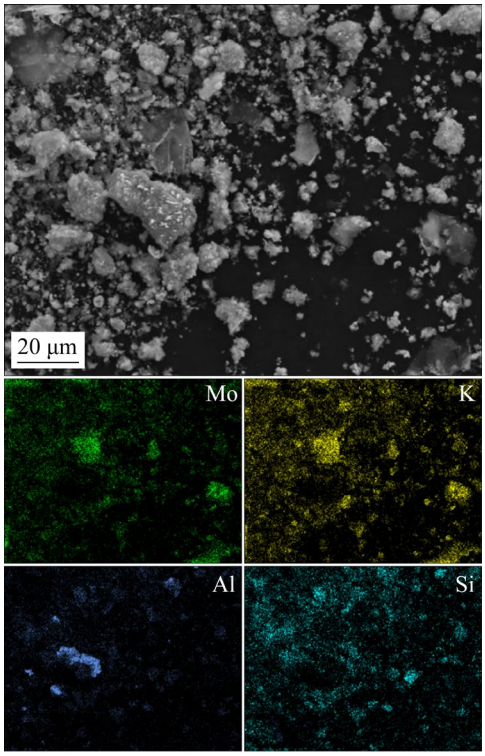


| Element | wt.% | at.% |
|---|---|---|
| Mo | 29.2 | 7.3 |
| K | 8.1 | 5.0 |
| Al | 5.6 | 5.0 |
| Si | 3.9 | 3.3 |

**Fig. 7** EDS spectroscopic analysis of water-leached residue

The optimal oxidative roasting conditions explored above were used to treat molybdenite #2, thereby achieving a leaching efficiency of 99.1% (slag rate: 3.4%), which proved that the ore adaptability of the method was relatively strong. Given the high-phosphorus (P) content, arsenic (As), silicon (Si), and other impurities contained in the molybdenite as well as the subsequent method were used in the molybdenite #2.

### 3.2 Impurity removal using potassium−magnesium salt method

After the oxidative roasting and subsequent KOH−water leaching, $SO_4^{2-}$, $PO_4^{3-}$, $AsO_4^{3-}$, $SiO_3^{2-}$, and $MoO_4^{2-}$ were all present in the leaching solution. Previous studies indicated that Mo was difficult to separate selectively from impurities such as $PO_4^{3-}$, $AsO_4^{3-}$, and $SiO_3^{2-}$ due to the hybridization effects. HE et al [30] demonstrated that $PO_4^{3-}$ was removed from tungstate solutions by adding Mg and ammonium salts while controlling the pH to precipitate $MgNH_4PO_4$. The radii of $NH_4$ and K were very similar, resulting in nearly identical solubilities of $MgNH_4PO_4$ and $MgKPO_4$ precipitates. Given the similar nature of W and Mo, the addition of Mg salts in the molybdate system also led to the formation of low-solubility precipitates such as $MgKPO_4$, which effectively removed impurities such as P, As, and Si. This method replaced the traditional ammonium−magnesium salt process for the impurity removal (Fig. 8).

In this experiment, $MgSO_4$ was utilized as the transition treatment agent, and various parameters including pH, temperature, Mg salt excess coefficient, and reaction time were optimized to enhance the formation of the MgKA (A= $PO_4^{3-}$, $AsO_4^{3-}$, and $SiO_3^{2-}$) phase, reaction selectivity, crystallization, and Mo−A separation selectivity. It also improved the Mo−A separation selectivity, reduced Mo loss, and obtained MgKA crystals. Given their similar properties of P, As, and Si, as well as the high P content required in the actual product, P was utilized as a representative impurity to illustrate the Mg salt precipitation and removal process.

The effects of pH, temperature, Mg salt excess coefficient, reaction time, and P content on the P removal efficiency were investigated. The Mo loss ratio was calculated under the corresponding conditions to investigate the optimal conditions for complete P removal. The experimental $K_2MoO_4$ concentration was 0.1 mol/L, with a 100 mL sample and stirring speed maintained at 200 r/min (Fig. 9).

The pH exhibited a significant influence on the removal efficiency. Subsequently, with P concentration of 0.3 g/L, and an excess $MgSO_4$ coefficient of 1.2, at 30 °C, the P removal efficiency was extremely low below pH 9, with minimal P separation from the system. When the pH was increased to a strongly alkaline value of 10, the P removal was significantly higher, reaching 91.61% at pH 11. As the pH continued to increase, the Mo loss ratio decreased, thereby affecting the P removal

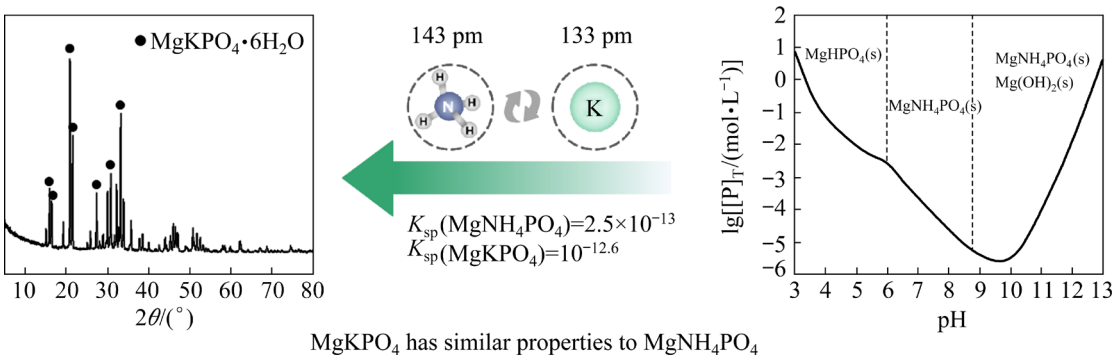


**Fig. 8** Principle diagram for P removal by magnesium salt precipitation in molybdate system [30]

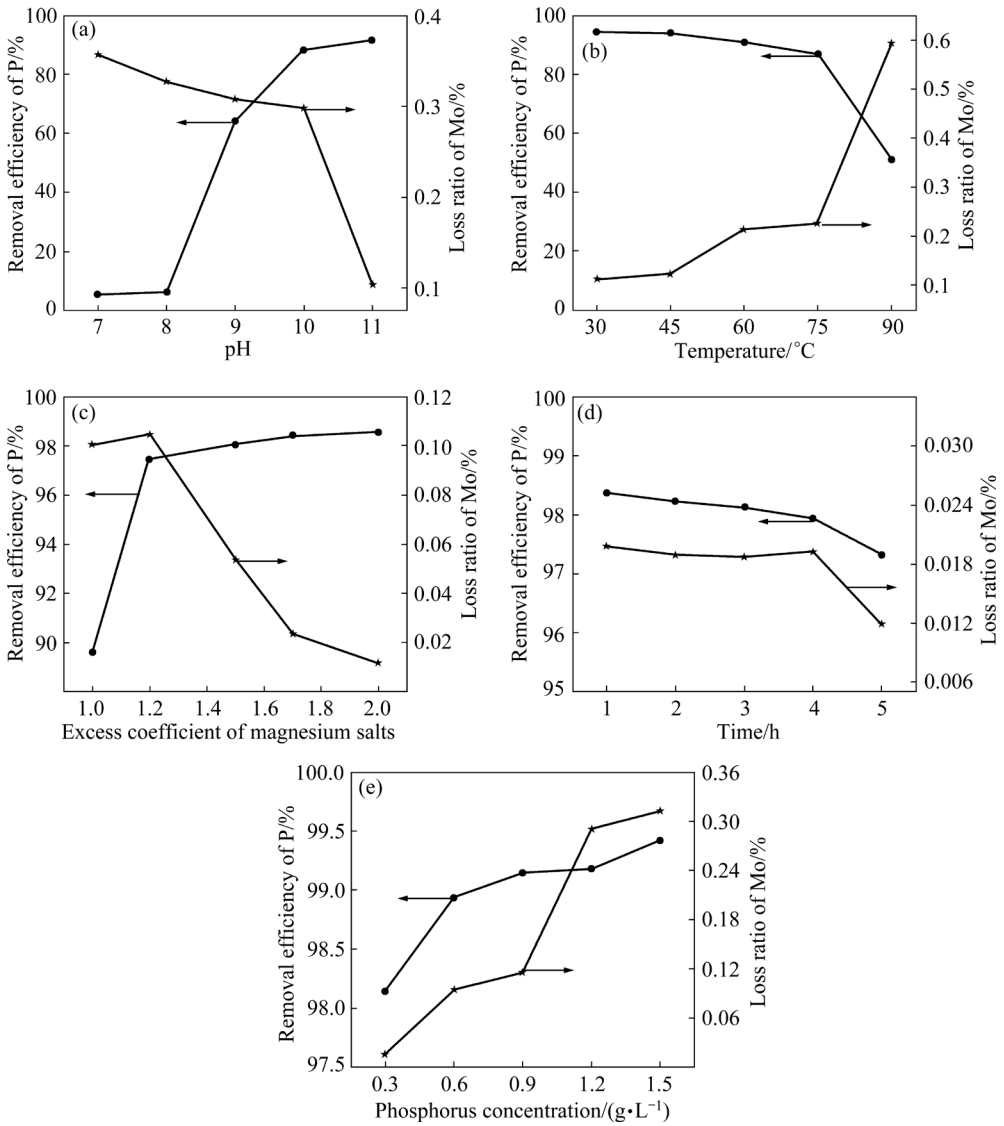


**Fig. 9** Effect of processing conditions on removal efficiency of P and loss ratio of Mo: (a) pH; (b) Temperature; (c) Excess coefficient of magnesium salts; (d) Time; (e) Phosphorus concentration

efficiency. Therefore, subsequent tests were conducted at pH 11 (Fig. 9(a)).

When the temperature was increased from 30 to 90 °C, the P removal efficiency decreased from 94.12% to 50.90% with increasing Mo loss ratio. The solubility of the $MgKPO_4$ precipitate increased progressively with increasing temperature, leading to the redissolution above 75 °C and a

significantly higher final P content, thereby diminishing the effectiveness of P removal. Consequently, the process was therefore conducted at room temperature, where the Mo loss ratio was only 0.11%, which was largely negligible (Fig. 9(b)).

The Mg salt excess coefficient was positively correlated with the P removal efficiency. The P removal efficiency increased accordingly and stabilized at 98.42% when the Mg salt excess coefficient reached 1.7. At this point, the Mo loss ratio was only 0.02%, and the P concentration in the system was reduced to $<2\times10^{-6}$. A further increase in Mg salt concentration was unnecessary. Therefore, a Mg salt excess coefficient of 1.7 was chosen for subsequent experiments (Fig. 9(c)). Time exhibited minimal influence on the removal process. Under optimal pH and temperature conditions, a white precipitate was observed immediately after adding the Mg salt, with only a slight decrease in the removal efficiency over time. This decrease was due to the inevitable mechanical movement of the stirring, which generated a small amount of heat that dissolved some of the precipitates. Prolonged stirring hindered stable nuclei growth, which led to partial redissolution (Fig. 9(d)).

Finally, the removal effect at different P concentrations was investigated to assess the adaptability of the method to different pyromorphite qualities. The results indicated that P removal efficiency remained relatively constant with different P concentrations. At high P concentrations, 99.42% of P was removed compared with 98.14% at 0.3 g/L, but this was accompanied by a small increase in Mo loss (Fig. 9(e)). This indicated that the Mg salt precipitation method is a straightforward, efficient, and effective approach for high-phosphorus product recovery. This method offered significant advantages over the traditional ammonium−magnesium salt P removal process. The XRD pattern and scanning electron microscopy (SEM) image of the Mg-containing precipitate are shown in Fig. 10.

The experimental results indicated that the optimal P removal conditions for a Mo simulant containing 0.3 g/L P were pH 11, 30 °C, and Mg salt excess coefficient of 1.7. Under these conditions, a removal efficiency of 98.37% was obtained after 1 h. Under the same conditions, the removal efficiency increased to 99.42% when the P content was 1.5 g/L. The Mo loss during this process was negligible and did not affect the subsequent preparation of the Mo product.

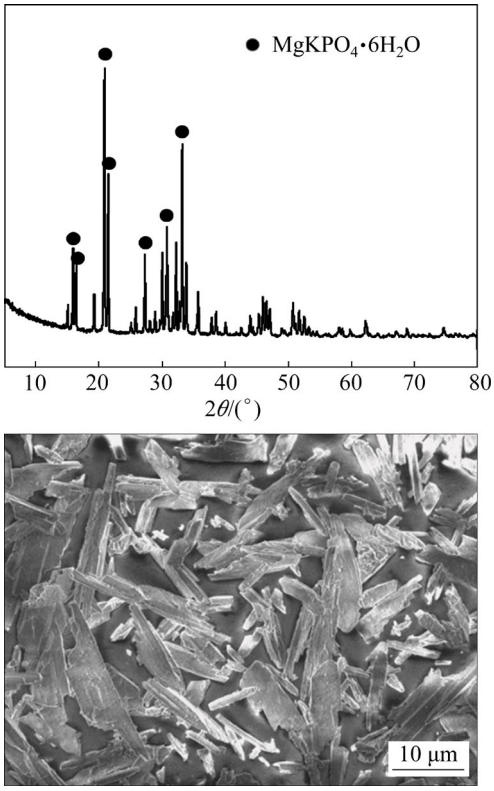


**Fig. 10** XRD pattern and SEM image of magnesium-containing precipitates

In the water-leaching process of calcined materials, the competition among $K_2MoO_4$, $K_2SO_4$, and KOH necessitated segmented water leaching to effectively separate $K_2MoO_4$ and $K_2SO_4$. This separation resulted in a high concentration $K_2MoO_4$ solution, which was subsequently purified through $MgSO_4$ addition. Upon controlling the above processing parameters, anion A ($PO_4^{3-}$, $AsO_4^{3-}$, and $SiO_3^{2-}$) relatively transformed into MgKA crystals. Subsequent solid–liquid separation resulted in a highly purified $K_2MoO_4$−$K_2SO_4$ solution, ensuring effective removal of As and Si in addition to P.

### 3.3 Preparation of polymolybdenum products

The simple and efficient extraction of Mo was achieved by adjusting the solution pH to influence degree of Mo polymerization, thereby affecting its tendency to form polyacid ions in a weakly acidic environment. As shown in Fig. 11, temperature, stirring speed, and time exhibited no significant effect on the crystallization efficiency of

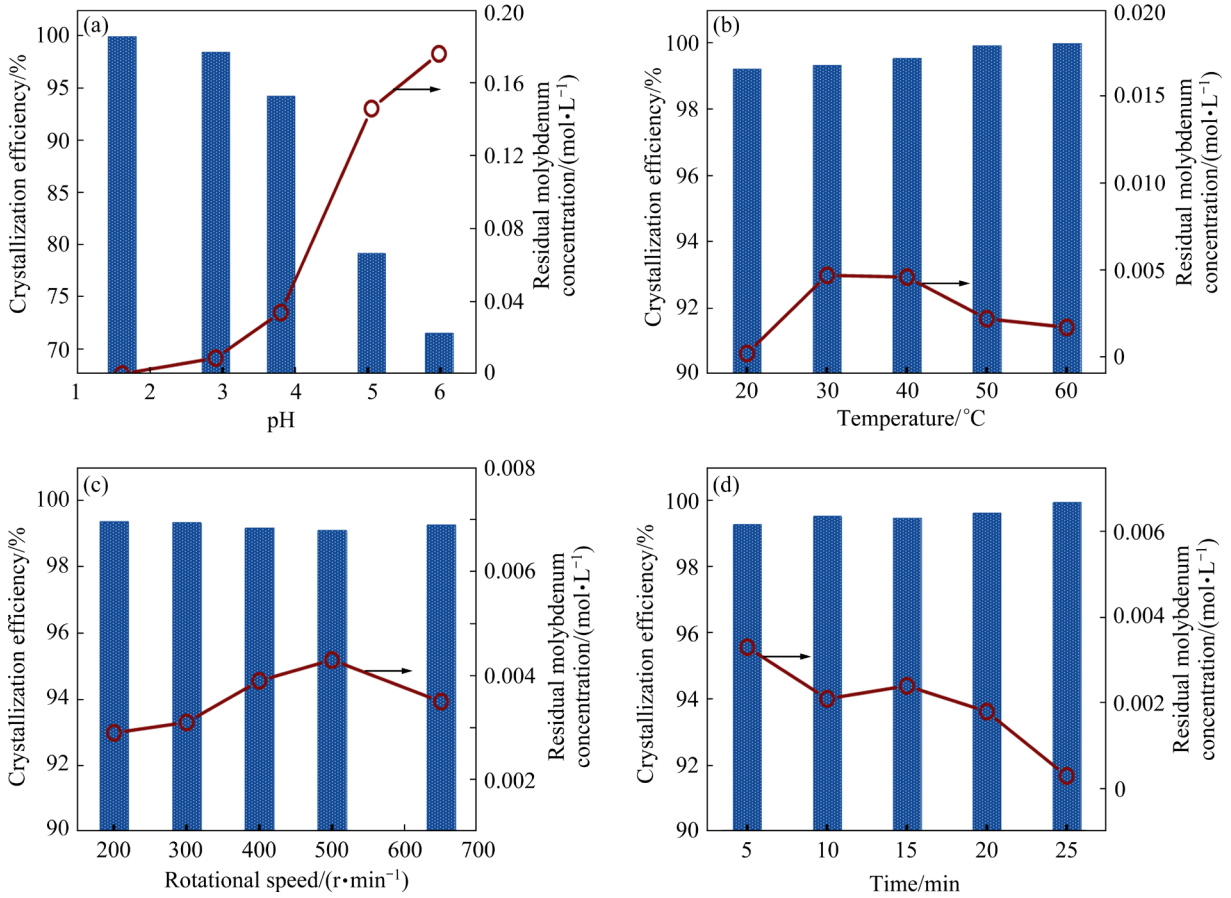


**Fig. 11** Effect of crystallization conditions on crystallization efficiency of Mo: (a) 20 °C, 200 r/min, 10 min; (b) pH 1.6, 200 r/min, 10 min; (c) pH 1.6, 20 °C, 10 min; (d) pH 1.6, 20 °C, 200 r/min

potassium polymolybdate. Conversely, different pH values significantly affected the polymerization of $MoO_4^{2-}$, with the crystallization efficiency decreasing with increasing pH values (Fig. 11(a)). In practice, crystallization did not occur under weakly alkaline conditions.

The polymerized $K_xMo_yO_z$ crystals and the mother liquor were produced upon adding $H_2SO_4$ to the purified $K_2MoO_4$−$K_2SO_4$ solution. Furthermore, XRD patterns of $K_xMo_yO_z$ crystals at different pH values are shown in Fig. 12. The molybdate exhibited a high degree of polymerization, particularly stable at low pH, with efficient crystallization and minimal residual Mo in the solution, thereby indicating suitability for acidic precipitation and crystallization at low pH values. Subsequently, during the acidification process of the $K_2MoO_4$ solution, Mo ions polymerized into various species with decreasing pH, including $MoO_4^{2-}$, $Mo_3O_{10}^{2-}$, $Mo_7O_{24}^{6-}$, $Mo_8O_{24}^{4-}$, etc. This corresponded to conventional methods for preparing various ammonium molybdate products through acid precipitation and crystallization [31,32]. Under the condition of pH 1, the predominant products were a mixture of potassium trimolybdate and potassium heptamolybdate.

### 3.4 Preparation of $K_2SO_4$ byproducts

The potassium and sulfate ions introduced were recovered in the form of $K_2SO_4$, which is a high-quality and efficient soluble potash fertilizer. It is also the primary raw material for the production of ternary compound fertilizers containing nitrogen (N), P, and K, thereby exhibiting a high recovery value. Because Mo is a trace element required for crop growth, Mo fertilizers are generally applied as a base, seed, and chasing fertilizer. Therefore, they are suitable for the preparation of $K_2SO_4$ agricultural fertilizer through $K_2MoO_4$ metallurgical system. This allowed for the recovery of S from minerals and the introduced K ions while minimizing the wastewater discharge. The XRD pattern in Fig. 13 showed that the final product was pure $K_2SO_4$ crystals. According to the Chinese National

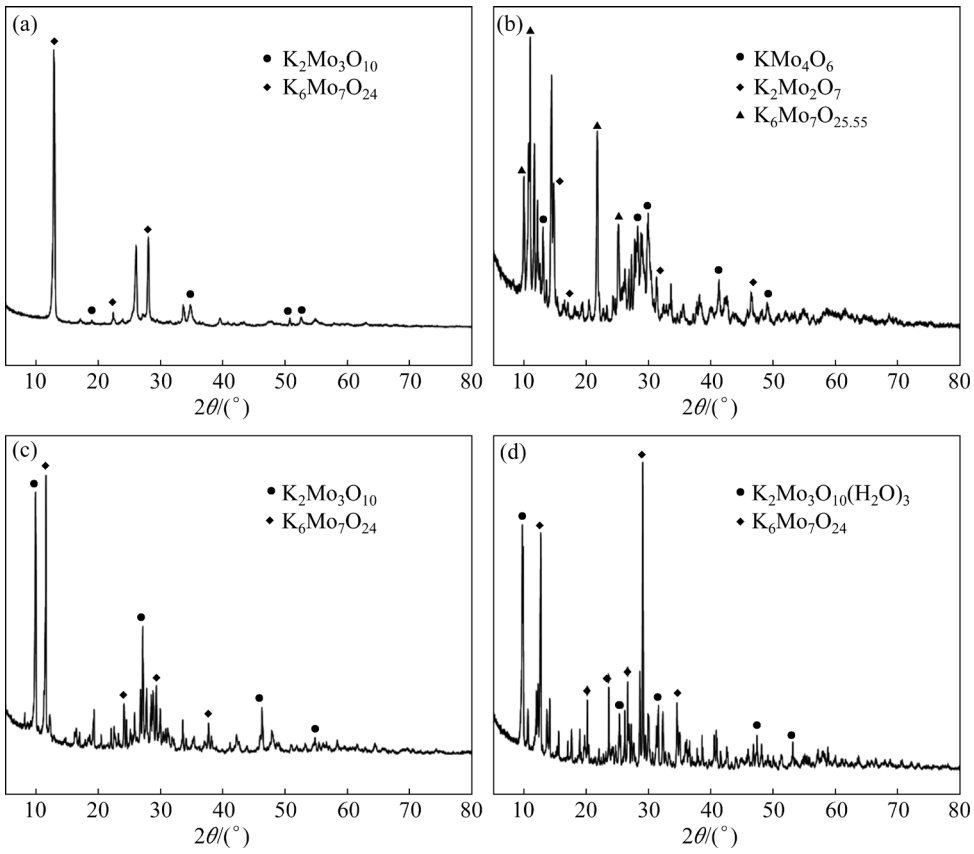


**Fig. 12** XRD patterns of polymerization products of $K_xMo_yO_z$ at different pH values: (a) pH 1; (b) pH 2; (c) pH 3; (d) pH 6

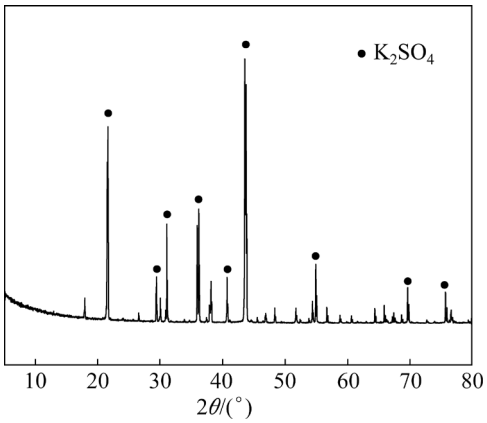


**Fig. 13** XRD pattern of potassium sulfate crystals

Standard GB/T 20406—2017 [33], the $K_2SO_4$ product obtained from this process has the following composition $w(K_2O)$=52.34%, $w(S)$=19.69%, $w(Cl^-)$=0.98%, $w(H_2O)$=0.69%, and $w(H_2SO_4)$=0.67%. This composition meets the agricultural requirements and exhibits high economic value (Table 3).

### 3.5 Flowchart of novel process for extraction of Mo from molybdenite

A new process for recovering Mo from molybdenite (Fig. 14) was proposed based on successful S fixation through oxidative roasting with KOH and the preparation of $K_xMoO_4$ through crystallization after Mg salt removal. This innovative approach not only addressed $SO_2$ treatment challenges but also efficiently recovered both Mo and S resources. The addition of a leaching agent further minimized wastewater discharge. Additionally, this process enhanced Mo product enrichment and offered a novel method for preparing potassium-doped ammonium molybdate and K−Mo bronze.

**Table 3** Requirements of $K_2SO_4$ for agricultural use and corresponding contents of sample (wt.%)

| Composition | Agricultural use (GB/T 20406—2017) | $K_2SO_4$ sample |
|---|---|---|
| $K_2O$ | ≥52.0 | 52.34 |
| S | ≥17.0 | 19.96 |
| $Cl^-$ | ≤1.5 | 0.98 |
| $H_2O$ | ≤1.0 | 0.69 |
| Free acid ($H_2SO_4$) | ≤1.0 | 0.67 |

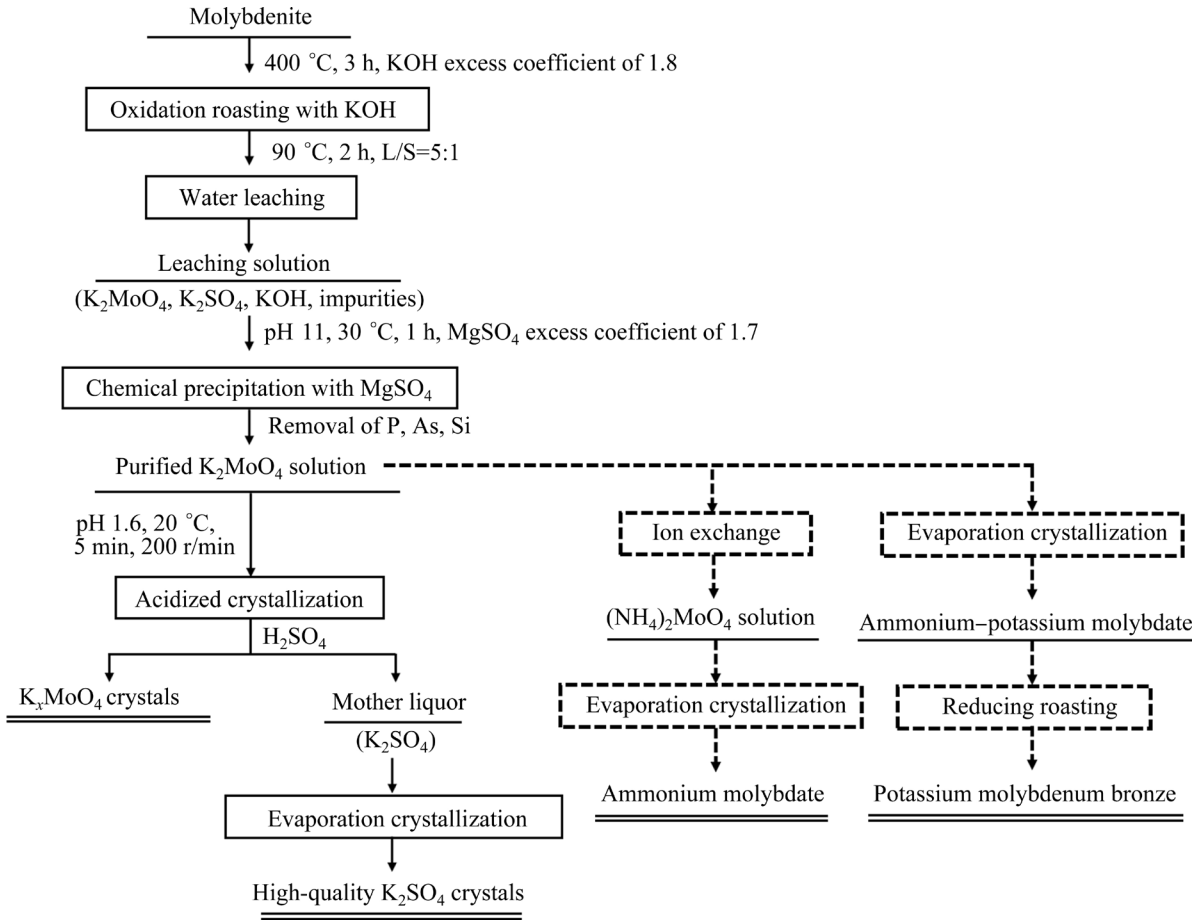


**Fig. 14** General flow chart of novel process for extraction of Mo from molybdenite

## 4 Conclusions

(1) Over 99.35% of Mo was water-leached from the molybdenum calcine, which was produced upon adding KOH at a roasting temperature of 400 °C, with a KOH excess coefficient of 1.8, and a roasting time of 3 h.

(2) The K−Mg salt precipitation method could be utilized to remove 98.37% of P from the leaching solution under a pH value of 11, a temperature of 30 °C, an Mg salt excess coefficient of 1.7, and a duration of 1 h.

(3) Over 99% of $K_xMo_yO_z$ polymerized crystals were produced when the pH of the purified $K_2MoO_4$ solution was adjusted to < 1.0 at 20 °C within 5 min. Additionally, $K_2SO_4$ was prepared through evaporative crystallization, thereby facilitating efficient utilization of K and S. This product was suitable for use as a $K_2SO_4$ fertilizer.

### CRediT authorship contribution statement

**Mu-ye CUI:** Conceptualization, Experimental investigation, Writing − Original draft; **Jiang-tao LI:** Conceptualization, Experimental investigation, Writing − Original draft; **Zhong-wei ZHAO:** Supervision, Writing − Review & editing; **Xu-heng LIU:** Methodology, Writing − Review & editing; **Xing-yu CHEN:** Funding acquisition, Writing − Review & editing; **Li-hua HE:** Experimental investigation, Writing − Review & editing; **Feng-long SUN:** Writing − Review & editing.

### Declaration of competing interest

The authors declare that they have no known competing financial interests or personal relationships that could have appeared to influence the work reported in this paper.

### Acknowledgments

This work was financially supported by the National Natural Science Foundation of China (No. 52174340), the National Key Research and Development Project of China (No. 2022YFC2904505), the Hunan FURONG Scholars Project and the Basic Science Centre of the National Natural Science Foundation of China (No. 72088101).

## References


[1] LIU Bing-bing, ZHANG Bei, HAN Gui-hong, WANG Mei-mei, HUANG Yan-fang, SU Sheng-peng, XUE Yu-bin, WANG Yi-Zhuang. Clean separation and purification for strategic metals of molybdenum and rhenium from minerals and waste alloy scraps—A review [J]. Resources Conservation & Recycling, 2022, 181: 106232. https://doi.org/ 10.1016/j.resconrec.2022.106232

[2] YI Gao-song, MACHA E, van DYKE J, MACHA R, MCKAY T, FREE M L. Recent progress on research of molybdenite flotation: A review [J]. Advances in Colloid and Interface Science, 2021, 295: 102466. https://doi.org/10.1016/j.cis.2021.102466

[3] LI Fei, CHEN Xing-yu, ZHANG Wen-juan, HE Li-hua, ZHAO Zhong-wei. Conversion of molybdenite by a mineral phase reconstruction method and leaching kinetics of its product [J]. International Journal of Refractory Metals and Hard Materials, 2017, 62: 14−20. https://doi.org/10.1016/j.ijrmhm.2016.10.010

[4] LI Xiao-bin, WU Tao, ZHOU Qiu-sheng, QI Tian-gui, PENG Zhi-hong, LIU Gui-hua. Kinetics of oxidation roasting of molybdenite with different particle sizes [J]. Transactions of Nonferrous Metals Society of China, 2021, 31: 842−852. https://doi.org/10.1016/S1003-6326(21)65543-7

[5] WANG Qian, LIU Chen-hui, ZHANG Li-bo, GAO Ji-yun, WANG Fang, DAI Ying. Preparation and mechanism of molybdenum trioxide by microwave oxidation roasting of molybdenite [J]. The Chinese Journal of Nonferrous Metals, 2022, 1−22. (in Chinese) https://doi.org/10.11817/j.ysxb.1004.0609.2022-43253

[6] ZHAO Zhi-peng, GUO Min, ZHANG Mei. Extraction of molybdenum and vanadium from the spent diesel exhaust catalyst by ammonia leaching method [J]. Journal of Hazardous Materials, 2015, 286: 402−409. https://doi.org/10.1016/j.jhazmat.2014.12.063

[7] LIANG Xin, TANG Jun-jie, LI Lai-shi, WU Yu-sheng, SUN Yuan. A review of metallurgical processes and purification techniques for recovering Mo, V, Ni, Co, Al from spent catalysts [J]. Journal of Cleaner Production, 2022, 376: 134108. https://doi.org/10.1016/j.jclepro.2022.134108

[8] WANG Lu, ZHANG Guo-hua, DANG Jie, CHOU Kuo-chi. Oxidation roasting of molybdenite concentrate [J]. Transactions of Nonferrous Metals Society of China, 2015, 25: 4167−4174. https://doi.org/10.1016/S1003-6326(15)64067-5

[9] ZHANG Meng-ping, LIU Chen-hui, ZHU Xiong-jin, XIONG Hua-bin, ZHANG Li-bo, GAO Ji-yun, LIU Man-hong. Preparation of ammonium molybdate by oxidation roasting of molybdenum concentrate: A comparison of microwave roasting and conventional roasting [J]. Chemical Engineering and Processing−Process Intensification, 2021, 167: 108550. https://doi.org/10.1016/j.cep.2021.108550

[10] GAO Bing-ying, JIANG Hao-hao, ZENG Man, PENG Ming-guo, HU Lin-chao, ZHANG Wen-yi, MAO Lin-qiang. High-efficiency recycling method for Mo and Ni from spent catalyst via soda roasting and solvent extraction [J]. Journal of Cleaner Production, 2022, 367: 143401. https://doi.org/10.1016/j.jclepro.2022.132976

[11] LI Xiao-bin, SHEN Lei-ting, ZHOU Qiu-sheng, PENG Zhi-hong, LIU Gui-hua, QI Tian-gui. Scheelite conversion in sulfuric acid together with tungsten extraction by ammonium carbonate solution [J]. Hydrometallurgy, 2017, 171: 106−115. https://doi.org/10.1016/j.hydromet.2017.05.005

[12] KHOSHNEVISAN A, YOOZBASHIZADEH H, MOZAMMEL M, SADRNEZHAAD S K. Kinetics of pressure oxidative leaching of molybdenite concentrate by nitric acid [J]. Hydrometallurgy, 2012, 111/112: 52−57. https://doi.org/10.1016/j.hydromet.2011.10.002

[13] WANG Si-fu, WEI Chang, DENG Zhi-gan, LI Cun-xiong, LI Xin-bing, WU Jun, WANG Ming-shuang, ZHANG Fan. Extraction of molybdenum and nickel from Ni−Mo ore by pressure acid leaching [J]. Transactions of Nonferrous Metals Society of China, 2013, 23: 3083−3088. https://doi.org/10.1016/S1003-6326(13)62837-X

[14] WANG Ming-shuang, WEI Chang, FAN Gang, LI Min-ting, DENG Zhi-gan, WANG Si-fu. Selective extraction of Mo from a Ni−Mo ore using pressure alkaline leaching [J]. Hydrometallurgy, 2015, 153: 6−11. https://doi.org/10.1016/j.hydromet.2015.01.008

[15] LIU Wei-ping, XU Hui, YANG Xi-yun, SHI Xi-chang. Extraction of molybdenum from low-grade Ni−Mo ore in sodium hypochlorite solution under mechanical activation [J]. Minerals Engineering, 2011, 24: 1580−1585. https://doi.org/10.1016/j.mineng.2011.08.010

[16] CAO Zhan-fang, WANG Ming-ming, ZHONG Hong, CHEN Na, XIA Liu-yin, FAN Fan, LIU Guang-yi, WANG Shu-ai. Purification of bismuthinite concentrate by selective electro-oxidation of molybdenite [J]. Hydrometallurgy, 2015, 154: 95−101. https://doi.org/10.1016/j.hydromet.2015.04.012.

[17] ZHOU Qiu-sheng, YUN Wei-tao, XI Jun-tao, LI Xiao-bin, QI Tian-gui, LIU Gui-hua, PENG Zhi-hong. Molybdenite–limestone oxidizing roasting followed by calcine leaching with ammonium carbonate solution [J]. Transactions of Nonferrous Metals Society of China, 2017, 27: 1618−1626. https://doi.org/10.1016/S1003-6326(17)60184-5

[18] SUN Hu, LI Guang-hui, WANG Jian, BU Qun-zhen, LUO Jun, RAO Ming-jun, PENG Zhi-wei, JIANG Tao. Short-flow preparation of pure $MoO_3$ from $CaCO_3$ added molybdenite concentrate pellet by sublimation with flue gas recirculation [J]. Journal of Cleaner Production, 2021, 284: 124747. https://doi.org/10.1016/j.jclepro.2020.124747

[19] SUN Hu, LI Guang-hui, BU Qun-zhen, FU Zhong-qiao, LIU Hui-bo, ZHANG Xin, LUO Jun, RAO Ming-jun, JIANG Tao. Features and mechanisms of self-sintering of molybdenite during oxidative roasting [J]. Transactions of Nonferrous Metals Society of China, 2022, 32: 307−318. https://doi.org/10.1016/S1003-6326(22)65796-0

[20] ZHANG Zheng-qing, HE Fang, ZHANG Yan-ling, YU Ru-jun, LI Ya-qi, ZHENG Zhi-lei, GAO Zhen-qiang. Experiments and modelling of potassium release behavior from tablet biomass ash for better recycling of ash as eco-friendly fertilizer [J]. Journal of Cleaner Production, 2018, 170: 379−387. https://doi.org/10.1016/j.jclepro.2017.09.150

[21] EISA E A, MELIGY M M , ZIEDAN H E. Application of

composts and potassium sulphate on root rot incidence, morphological growth, yield components, oil content and constitutes of marjoram plants (*Majorana hortensis L.*) [J]. Biocatalysis and Agricultural Biotechnology, 2022, 42: 102334. https://doi.org/10.1016/j.bcab.2022.102334

[22] CHAO Xi, ZHANG Ting-an, LV Guo-zhi, ZHAO Ai-chun, LIANG Zhi-peng, LIN Sheng-nan, CHEN Yang, ZHAO Qiu-yue, CHENG Fang-qin. A novel process for one-step preparing potassium-containing fertilizer using red mud or CFA synergistic extraction of alumina [J]. Process Safety and Environmental Protection, 2022, 167: 443−453. https://doi.org/10.1016/j.psep.2022.09.037

[23] WANG Yong, Gao Jia-cheng, Chen Gong-ming, LI Wei-qin, ZHOU Yong-gui, ZHANG Wei. Properties at elevated temperature and recrystallization of molybdenum doped with potassium, silicon and aluminum [J]. International Journal of Refractory Metals and Hard Materials, 2008, 26: 9−13. https://doi.org/10.1016/j.ijrmhm.2007.01.009

[24] CHIN K, EDA K, SOTANI N. Hydrothermal synthesis of the blue potassium molybdenum bronze, $K_{0.28}MoO_3$ [J]. Journal of Solid State Chemistry, 2002, 164: 81−87. https://doi.org/10.1006/jssc.2001.9450

[25] NISHIDA T, EDA K. Hydrothermal preparation of blue molybdenum bronze nanoribbons: Structural changes in mother crystals, related to solid-state conversion and crystallite splitting to nanomorphology [J]. Journal of Nanoparticle Research, 2018, 20: 27. https://doi.org/10.1007/s11051-018-4134-5

[26] NISHIDA T, EDA K, TAKAHASHI K, SAKURAI T, OHTA H, WHITTINGHAM M S. Preparation of nanoribbons of blue potassium molybdenum bronze [J]. Chemistry Letters, 2013, 42: 1514−1516. https://doi.org/10.1246/cl.130792

[27] IHSAN B. Thermochemical data of pure substances [M]. VILEY Online Library, 2008. https://doi.org/10.1002/9783527619825.ch3

[28] LI Zhong-rui, JIANG Ming, FU Yi-lu. XPS of the surface species in sulfided Mo−K−Rh/$Al_2O_3$ catalysts Chinese [J]. Journal of Chemical Physics, 1997, 10: 50−53. (in Chinese)

[29] CHE Jian-yong, ZHANG Wen-juan, MA Bao-zhong, WANG Cheng-yan. An efficient process for recovering copper as CuO nanoparticles from acidic waste etchant via chemical precipitation and thermal decomposition: Turning waste into value-added product [J]. Journal of Cleaner Production, 2022, 369: 133404. https://doi.org/10.1016/j.jclepro.2022.133404

[30] HE Gui-xiang, HE Li-hua, ZHAO Zhong-wei, CHEN Xing-yu, GAO Li-li, LIU Xu-heng. Thermodynamic study on phosphorus removal from tungstate solution via magnesium salt precipitation method [J]. Transactions of Nonferrous Metals Society of China, 2013, 23: 3440−3447. https://doi.org/10.1016/S1003-6326(13)62886-1

[31] CHEN Chao, ZHANG Gui-qing, GUAN Wen-juan, WU Xin-sheng, WU Sheng-xi, LI Qing-gang, CAO Zuo-ying. Study on a new process for the wet preparation of ammonium heptamolybdate from ammonium dimolybdate [J]. Rare Metals and Cemented Carbides, 2023, 51(2): 15−19. (in Chinese) https://doi.org/10.19990/j.issn.1004-0536.2023.02.013.07.

[32] LI Jiang-tao, LUO Yong-jin, LI Zhi-chao, ZHAO Zhong-wei, LIU Xu-heng, CHEN Xing-yu, HE Li-hua, SUN Feng-long, ZHANG Ning. Precise control and continuous production ofβ-ammonium tetramolybdate in concentric reactor [J]. Transactions of Nonferrous Metals Society of China, 2024, 34: 309−321. https://doi.org/10.1016/S1003-6326(23)66400-3

[33] GB/T 20406—2017. The standard test method of potassium sulfate for agricultural use [S]. (in Chinese)

# 基于辉钼矿矿相水溶性转化的钼冶金新工艺

崔慕野[1]，李江涛[1,2]，赵中伟[1,2]，刘旭恒[1]，陈星宇[1]，何利华[1]，孙丰龙[1]

1. 中南大学 冶金与环境学院，长沙 410083；
2. 中南大学 稀有金属冶金与材料制备湖南省重点实验室，长沙 410083

**摘　要：**采用 KOH 氧化焙烧辉钼矿的方式将矿物中的钼和硫转化为水溶性的 $K_2MoO_4$ 和 $K_2SO_4$。在 400 ℃、加入理论量 1.8 倍的 KOH 和焙烧 3 h 的条件下氧化焙烧辉钼矿，然后再经水浸提取钼，钼的浸出率超过 99%。采用钾镁盐沉淀法净化浸出液。在 pH 11、温度 30 ℃、镁盐过量系数 1.7、反应时间 1 h 的条件下，可去除 $K_2MoO_4$ 溶液中 98.37%的磷杂质。当溶液 pH 调至 1 时，净化后的溶液中钼的结晶率达到 99%以上。随后，结晶母液中的 S 和 K 浓缩得到硫酸钾农肥。该方法实现了辉钼矿的清洁生产和钼、硫的高效回收。

**关键词：**辉钼矿；固硫焙烧；磷酸钾镁；多钼酸钾

**(Edited by Bing YANG)**